Synthesis of Stabilized Iron Nanoparticles from Acid Mine Drainage and Rooibos Tea for Application as a Fenton-like Catalyst

Elyse Kimpiab, Kashala Fabrice Kapiamba,* Leo Folifac, Oluwaseun Oyekola, and Leslie Petrik*
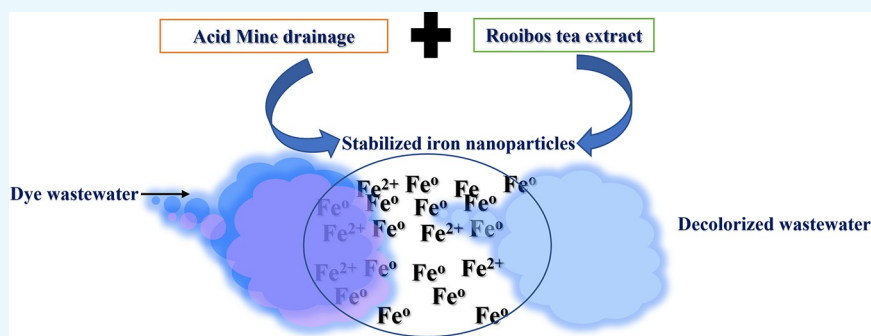
Read Online

ACCESS | Metrics & More | Article Recommendations

ABSTRACT: Intensive mining activities generate toxic acid mine drainage (AMD) effluents containing a high concentration of metals, including iron. The chemical synthesis of iron nanoparticles from this waste could lead to further environmental concerns. Therefore, the green synthesis of nanoparticles using plants has gained significant interest because of several benefits, including being eco-friendly. The current study reports a novel approach involving the synthesis of stabilized iron nanoparticles from AMD using rooibos tea extract. An aqueous solution of rooibos tea was prepared and titrated with AMD to reduce Fe^{2+}/Fe^{3+}. The samples synthesized under optimum conditions were characterized by TEM, XRD, FTIR, UV−Vis, and EDS. The results revealed that the nanoparticles had an average particle size of 36 nm with a spherical shape. These particles showed promising application as a Fenton-like catalyst for the degradation of textile dye (orange II sodium salt) with a removal efficiency of 94% within 30 min. Thus, the stabilized iron nanoparticles synthesized here performed in higher ranges than the currently reported Fenton-like catalysts regarding dye removal efficiency and reaction time.

1. INTRODUCTION

Mining industries are significant contributors to many countries' national gross domestic products.[1,2] Consequently, the huge amount of waste from mining activities adversely affects ecosystems, including human health.[3,4] Minerals are extracted from both open-pit and underground mine configurations across the life of the mine, inevitably leading to the generation of acid mine drainage (AMD), a toxic waste effluent. AMD is generated by the spontaneous oxidation of FeS_2 when exposed to air and water. On one hand, AMD can cause deleterious effects on the environment when discharged into water systems. Notably, AMD results in river pollution, depletion of aquatic life, and contamination of the food chain by toxic metals. The impacts of AMD, including the contamination of surface water, its threat to the quality of freshwater resources, and its impact upon the well-being of humans and the environment at large, are well documented.[5,6] Meanwhile, AMD has been chemically treated to precipitate metals, including iron, using reducing reagents. AMD remediation and prevention, treatment technique options, and resource recovery have been reviewed.[7,8] On the other

hand, the textile industry, which employs large amounts of colorants including dyes and dye-protecting agents, generates a huge amount of dye wastewater that is toxic to the environment.[9,10] This toxicity may range from soil contamination to pollution of an entire river, potentially causing severe harm to aquatic life. In many countries, the law recommends treating dye wastewater before its discharge into the environment and emphasizing decoloration. Adsorption techniques for purifying wastewater have become more prevalent in recent years owing to their efficiency in removing pollutants that are difficult to treat using biological methods. Adsorption can produce high-quality water and is an economically feasible process. Possible approaches to textile wastewater, including

24423

advanced oxidative and biological processes, have been critically reviewed.[11−13] Meanwhile, most currently employed approaches suffer from waste management and environmental protection setbacks, considering the life cycle of chemicals used, high cost, and technological immaturity for biological processes. Nevertheless, in recent years, environmental research has paid particular attention to zero-valent iron (ZVI) owing to its inherent reactivity to textile effluents such as dyes and site remediation applications.[14,15] For instance, orange II sodium salt is an azo dye produced by the azo coupling of *β*-naphthol and the diazonium derivative of sulfanilic acid. This dye is often used to dye wool in the textile industry. Furthermore, orange II sodium salt in wastewater is of specific environmental concern because it generates an unpleasant color to the water in addition to the hazards of dangerous by-products generated through oxidation, hydrolysis, or other chemical reactions occurring in the waste phase. Fenton-like reactions are responsible for the degradation of pollutants. Several studies have reported the mechanisms underlying these reactions. However, the activity of most heterogeneous catalysts decreases under macroneutral conditions due to strong dependence on the pH of the solution.[16] However, Yan et al.[17] recently provided a cocatalytic heterogeneous Fenton ($CoFe_2O_4/MoS_2$) system independent of the surrounding pH, thus enhancing the remediation of organic pollutants. Furthermore, Ji et al.[18] developed self-producing reactive oxygen species systems (made of a mixture of a cobalt-based catalyst Fe^{2+} species) and maintained the continuous and effective degradation of organic pollutants. Another type of catalyst that has shown immense success for pollutant degradation in water is ZVI nanoparticles (nZVI). These nanoparticles are predominantly 10−60 nm in size with exceptional characteristics and a maximum wavelength of 400 nm.[19−21] Shahwan et al.[22] reported that the higher surface reactivity of nZVI is due to its small size, large surface area, and oxidation state. The chemical synthesis of nZVI has been successfullyachieved by several groups; the synthesis methods, applications, and performance assessment of these nanoparticles have been well documented.[23−25] The major setback and the challenge in producing high volumes of iron nanoparticles using chemical methods relies on the need for NaBH4 as a reducing agent, which is very expensive and has strict environmental restriction policies. Hence, alternative "green" ways with the use of plant extracts or cheaper reducing agents have gained popularity in the past decade. Plant extracts have been proven to be impeccable reducing agents, and iron nanoparticles, including nZVI, were successfully synthesized.[26,27] The latest studies worth mentioning include the *Ricinus communis* aqueous seed extract used to synthesize nZVI to treat methylene blue-polluted water.[27] The other plant extracts explored as reductants comprise (list is nonexhaustive) onion peel extract, pomegranate peel extract, and *Cleistocalyx operculatus* leaf extract.[28−30]

The iron nanoparticles synthesis demonstrated in the abovementioned publications required manufactured chemicals (iron salts) as the source of iron. However, green reducing agents have been employed, thus only partially solving an eventual environmental concern. Considering that AMD contains a high concentration of iron which can be valorized, investment in effective technologies to recycle/reuse iron in AMD would promote sustainable economies. Thus, the recovery of iron from AMD could promote a circular economy.

Because of the limitations of chemical precipitation methods as well as potential environmental concerns, this research focused on synthesizing iron nanoparticles from AMD using rooibos tea extract (*Aspalathus linearis* or red tea) as a reducing reagent. This study avoids the chemical removal of iron, potentially resulting in secondary pollution. Here, an environmentally friendly alternative was employed to synthesize polyphenol-stabilized iron nanoparticles from AMD waste effluent using rooibos tea extract (RBE), a readily available resource. Furthermore, the effectiveness of the synthesized iron nanoparticles as a Fenton catalyst to remove orange II sodium salt from textile wastewater was assessed.

2. METHODOLOGY

2.1. Synthesis of Iron Nanoparticles. Fresh dry rooibos tea leaves (200 g) were added to 200 mL of a 20% ethanol solution (50% grade, Sigma-Aldrich) and then stirred for 1 h. Next, the liquid was separated from the tea leaves using a sieve, frozen, and dried for 72 h in a freeze dryer (−55 °C and 0.2 bar, FreeZone 2.5 L, Labconco). The dry powdered rooibos tea extract (about 15 g) obtained by freezing was mixed with 100 mL of distilled water to prepare solutions with a water concentration range of 5−20 g/L. The pH of the solution was measured before titration and varied in the range of 4 to 7 by adding drops of sodium hydroxide (NaOH) at room temperature. Finally, the pH-adjusted aqueous tea solution was poured into a burette for titration with 100 mL of AMD (from a coal mine in Mpumalanga, South Africa) using a magnetic stirring plate in the absence of oxygen (in a nitrogen-filled glove box). The raw AMD used in this study contained 100.30 mg/L of dissolved iron; the concentrations of other elements are presented in Figure 1.[31]
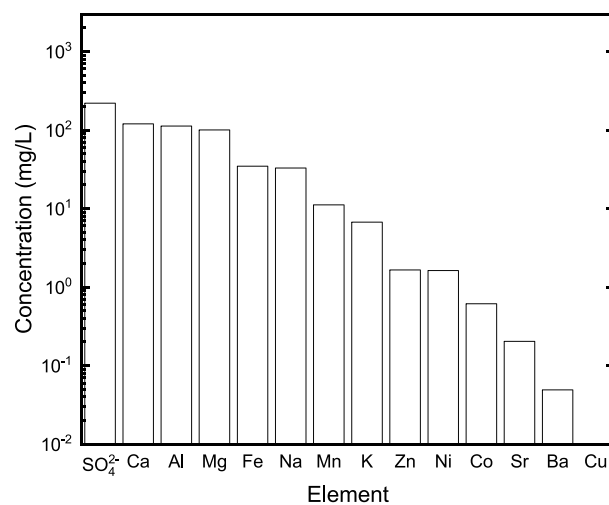

Figure 1. Elemental composition of AMD.

Reaction times of 0 to 24 h were evaluated to synthesize iron nanoparticles using rooibos tea extract as a vital parameter for optimization. The suspensions formed were centrifuged for 30 min to recover black pellets, which were washed with diluted ethanol and centrifuged for an additional 30 min. Finally, the washed black pellets were placed in a freeze-dryer for 72 h and characterized thereafter. The samples at various parameters were synthesized using a non-formal model as summarized in Table 1.

Table 1. Summary of Prepared Samples

sample code		concentration of RBE (g/L)	time (h)	pH	fixed parameters
EK 1	1	5	24	7	temperature (ambient), time, pH
	2	10			
	3	15			
	4	20			
EK 2	1	5	0	7	RBE concentration, pH, temperature (ambient)
	2		6		
	3		12		
	4		24		
EK 3	1	5	6	4	RBE concentration, time, temperature (ambient)
	2			4.5	
	3			5	
	4			5.5	
	5			6	
	6			7	

2.2. Ferric Reducing/Antioxidant Power Assay.

Ferric reducing/antioxidant power (FRAP) activity was measured according to the method developed by Benzie and Strain[32] with some modifications. Briefly, an acetate buffer (300 mM, pH 3.6) was mixed with a solution of 10 Mm TPTZ (2,4,6-tripyridyl-s-triazine) in 0.1 M HCl and $FeCl_3 \cdot 6H_2O$ (20 mM) in a ratio of 10:1:1 to obtain the working FRAP reagent. Then, 2 mg/ L each of ascorbic acid (standard) and plant extract were carefully prepared and subjected to agitation for 5 min with a vortex mixer (Dragon LAB MX-S) followed by centrifugation (Eppendorf centrifuge 5810R) at 1000 rpm for another 5 min to allow the formation of clear solutions of the test samples. Next, 100 mL of tea leaf extracts were mixed separately with 300 mL of the prepared FRAP reagent. The sample absorbance was measured at 593 nm with the Multiskan spectrum (Thermo Electro Corporation, MA, USA). Finally, methanol solutions of $FeSO_4 \cdot 7H_2O$ ranging from 100 to 2000 μM were prepared and used for creating the calibration curve of known Fe^{2+} concentration. The parameter equivalent concentration is defined as the antioxidant concentration having a Ferric-TPTZ reducing ability equivalent to 1 Mm $FeSO_4 \cdot 7H_2O$.

2.3. Characterization.

The prepared iron nanoparticles were characterized using a Hach Instruments DR6000 UV–Vis spectrometer (Hach Lange GmbH, Düsseldorf, Germany) in the wavelength range of 350–800 nm with a resolution of 1 nm. In addition, RBE and iron nanoparticles, prepared under optimum conditions (RBE = 5 g/L synthesized at room temperature, pH = 6, for 6 h of reaction time, sample EK35), were further characterized by Fourier transform infrared spectroscopy (FTIR, PerkinElmer PE1600). For FTIR analysis, samples were prepared by mixing 1% EK35 specimen with 100 mg of KBr powder and then compressing the mixture into a disc. A resolution of 2 cm^{-1} was employed, and an average of 32 scans were collected.

The morphology and dispersion of the prepared iron nanoparticles were characterized using transmission electron microscopy (TEM, Tecnai TF20 HRTEM). The images of the samples were recorded in bright-field mode operating at 5 kV. The size of the nanoparticles prepared at different pH values was measured using ImageJ software (National Institutes of Health, Bethesda, MD, USA) on TEM images. In addition, the localized elemental composition of the iron nanoparticles was determined in duplicate by electron dispersive spectroscopy (EDS, Oxford Instruments Aztec Energy EDS Analysis System) in conjunction with TEM.

X-ray diffraction (XRD) patterns of the iron nanoparticles were obtained using a D8 Advance XRD instrument (Bruker AXS, Germany) with a high-power Cu K$_\alpha$ radiation source (λ = 0.154 nm) at a voltage and current of 40 kV and 40 mA, respectively. All samples were scanned in steps from 10 to 80° 2θ at a scanning rate of 3° 2θ per minute.

2.4. Application of the Synthesized Iron Nanoparticles Using Orange II Sodium Salt.

The synthesized nanoparticles were applied as a Fenton-like catalyst to treat simulated dye wastewater. Batches were prepared by adding 40 mL of 50 ppm orange II sodium salt (85% dye content, Sigma-Aldrich) with 5 mL of hydrogen peroxide (50% solution, Sigma-Aldrich). A series of dosages of iron nanoparticles was added to the solution, and the mixtures were stirred for 30 min. The removal efficiency was measured using ultraviolet and visible spectrophotometry (UV–Vis) and compared to the removal efficiency of dye wastewater treated with hydrogen peroxide alone, a run treated as the control parameter. These experiments were performed in triplicate. The removal efficiency was calculated using the following equation:

$$\text{removal efficiency} = \frac{C_o - C_f}{C_o} \times 100$$

where C_o and C_f are initial and final dye concentrations, respectively.

3. RESULTS AND DISCUSSION

3.1. Antioxidant Activity of Some Selected Reductants.

The FRAP values of plant extracts often used for iron nanoparticles are shown in Table 2 on a dry weight basis of the sample.

Table 2. FRAP Values of Common Plant Extracts Used for the Synthesis of Iron Nanoparticles

plant and chemical reductants	FRAP per dry weight of the sample (μmol FeII/g)	COV (%) for triplicate measurement
green tea extract	888	1.89
green rooibos tea extract	805	2.41
rooibos tea extract	756	2.39
sodium borohydride	6014	2.72

From Table 2, it could be noticed that the FRAP values of the aqueous–ethanolic extracts of green tea, green rooibos tea, rooibos tea, and sodium borohydride were 805, 888, 756, and 6014 μmol/g, respectively. The sodium borohydride FRAP test value was compared with the tea extracts' antioxidant strength. Even though sodium borohydride had the highest FRAP value, the antioxidant values of the tea reductants were comparable. The aqueous–ethanolic polyphenolic tea extracts did not show significant discrepancies in their FRAP values. Therefore, all the tea extracts had a similar reducing capability of iron. It was further noticed that green tea had the highest FRAP value among the tea extract reductants. This was an indication that green tea had a greater capacity to reduce iron from a higher oxidation state to a lower oxidation state. The FRAP test findings suggest that tea extracts contain high amounts of polyphenolic compounds with the potential to act

as a reducing agent. It was expected that compounds that donate electrons to reduce Fe^{3+} to Fe^{2+} could also quench free radicals. In this line of investigation, the radical scavenging activity of the tea extracts was determined against the stable free radical DPPH (2,2-diphenyl-1-picrylhydrazyl) antioxidant activities.

3.2. Optimum Conditions for the Synthesis of Iron Nanoparticles.
In this study, by visual inspection, we observed a change in the solution color from light (AMD) to dark brown over time during treatment with rooibos tea extract. After 6 h, the reaction mixture turned from dark brown to black, and the nanoparticles appeared. The reaction was allowed to continue for up to 24 h, but only imperceptible color variation could be detected (see Figure 2). This
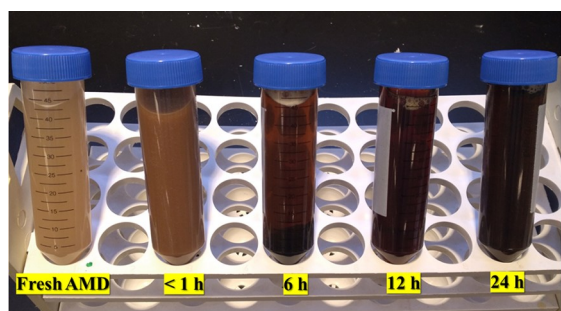

Figure 2. Color variation during AMD titration with Rooibos tea extract.

observation was similar to that reported by Kuang et al.[33] who reported that 6 h is generally sufficient to reduce iron from the AMD; thus, 6 h was deemed the optimum reaction time for the synthesis of all samples.

Experimental results showed that the size of the iron nanoparticles was significantly dependent on the pH at which the synthesis was conducted. For example, Figure 3 shows that iron nanoparticles synthesized in series EK3 were larger when formed at a pH range of 4 to 5 and relatively smaller at pH 6 (the optimum condition). The particle size was measured using ImageJ software on TEM images.
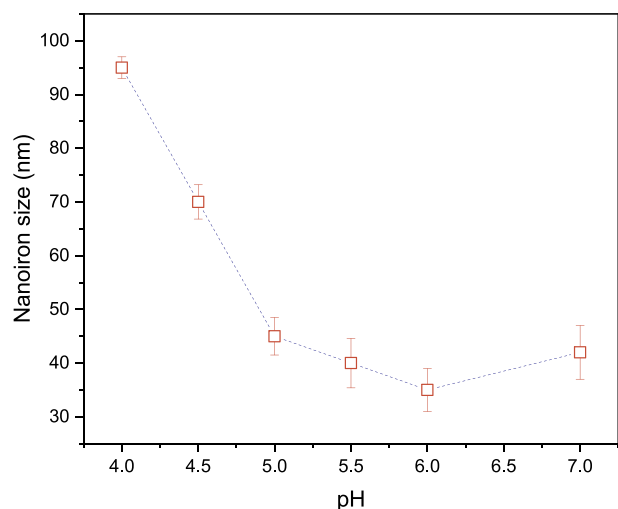

Figure 3. Effects of pH on particle size (prepared at room temperature and 6 h reaction time; EK3 series).

The lowest RBE concentration (5 g/L) corresponds to the literature as the optimum dosage for generating spherical particles.[34]

3.3. Characterization of Prepared Iron Nanoparticles.
The iron nanoparticles synthesized under optimum conditions (pH = 6; dosage of Rooibos tea = 5 g/L; reaction time = 6 h) were characterized by TEM, XRD, FTIR, UV−Vis, and EDS. Nanoparticles prepared under the above conditions had smaller average particle sizes (36.33 nm), providing a higher surface area for reaction and required a lower RBE concentration and minimum preparation time. UV−Vis spectra (Figure 4) were used to ascertain the existence of iron
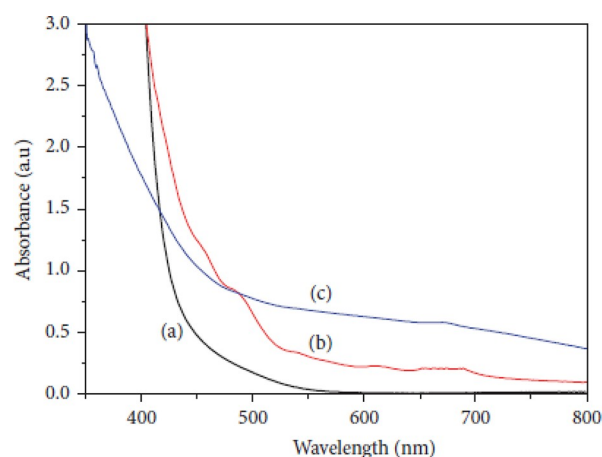

Figure 4. UV spectra of AMD (a), RBE (b), and iron nanoparticles (c); sample EK35.

nanoparticles with an absorption peak maximum in the range of 400−800 nm. Iron nanoparticles (Figure 4c) showed absorption at higher wavelengths. AMD (Figure 4a) showed no sharp absorption between 550 and 800 nm, while the rooibos tea itself (Figure 4b) showed a peak at 500 nm.[22] The differences in spectra between raw materials (RBE and AMD) and prepared nanoparticles illustrate the successful synthesis of nanoiron. Further details on the structure and composition are provided in the following characterizations.

The FTIR spectrum of rooibos tea (Figure 5a) displayed stretching vibrations at 3360 cm^{-1} for O−H and 1610 cm^{-1} for C=C. Absorption bands at 2900 and 1350 cm^{-1} for C−H and C−N groups, respectively.

In comparison with RBE, the FTIR spectrum of iron nanoparticles (Figure 4b) showed a stretch of the O−H group at 3400 cm^{-1}, C−H at 2900 cm^{-1}, C=C at 1630 cm^{-1}, and respectively, C−O−C and C−N at 1020 and 1375 cm^{-1}, which fitted well to the spectrum of RBE, showing that RBE stabilized the iron and suggesting that the surface of the synthesized nanoiron is primarily iron at higher oxidation states.[35,36] The O−H band is ascribed to the formation of lepidrocte (γ-FeOOH) on the surface of the presumed zero-valent core as confirmed by XRD. The functional group bands obtained in the FTIR spectrum of iron nanoparticles were similar to those reported in the literature for nZVI. The bonding of the oxidized polyphenols from RBE on the surface of iron nanoparticles was thus confirmed, and the results were in agreement with Hoag et al.,[34] such that the polyphenols present in rooibos tea, as in most plant extracts, could function as a powerful stabilizing and reducing agent responsible for the partial reduction of Fe^{2+}/Fe^{3+} to Fe^0. The morphology and size
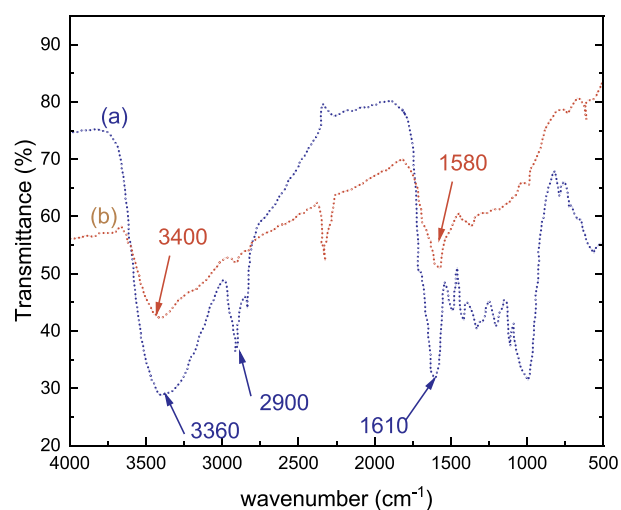
Figure 5. FTIR spectra of RBE (a) and synthesized iron nanoparticles (b), sample EK35.

of the EK35 sample appeared to show the formation of spherical particles enveloped in the polyphenol chain structures and a greater degree of dispersion. A reduction in the surface magnetism was observed when a magnet was used to separate iron nanoparticles in the slurry; it was only somewhat effective. Filtration was therefore used to assist magnetic separation.

Figure 6 shows the TEM image and XRD pattern of the iron nanoparticle sample prepared under optimum conditions (sample EK35). Using ImageJ (from TEM images), the average particle size was found to be 36 nm, and TEM revealed the existence of polyphenols in tea, partially coating the surface of the nanoiron. In terms of magnetism and dispersion, the results differed from those of Kuang et al.,[33] and the source of iron might be the reason for the discrepancy; Kuang et al. used iron salts' $FeCl_3$, while AMD was used as the source of iron in the current study. The nature and structure of the dissolved iron in AMD is worth further investigation. An inspection of the XRD spectrum of sample NK35 reveals peaks at 43.1 and 58 °, likely indicating the presence of Fe^o in its crystalline form.[36,37] It also displayed a peak at approximately 17.6°, identified as polyphenols found in the RBE. Similar observations have been reported in studies on the synthesis of iron nanoparticles using aqueous sorghum bran extracts and

three tea extracts (green tea, black tea, and oolong tea).[33,38] The peak at approximately 24.5° was attributed to iron hydroxides (FeOOH), whereas the maghemite (γ-Fe_2O_3) peak was observed at approximately 35.5°.[39,40] It is important to note the higher peak intensities for iron oxides and from the XRD patterns, which can be attributed to the fact that the iron nanoparticles synthesized by RBE were not all fully reduced metals as they existed as core/shell particles.

The elemental composition of sample EK35 displayed a pattern in the form of peaks of C, S, and K in addition to Fe and O. Carbon originated predominantly from the polyphenols found in rooibos tea, whereas Fe and S originated from AMD. Moreover, potassium (K) was attributed to Rooibos tea as it is vital to plant growth and exists in every living plant cell. The lower iron content observed may be due to the large mass percent of carbon from the polyphenol coating from RBE as was noticeable in the TEM images.[41]

Average atomic percentages obtained from EDS were 51.04 ± 0.49% for C, 23.15 ± 0.27% for O, 17.33 ± 0.17% for Fe, 6.10 ± 0.04% for K, and 2.39 ± 0.14% for S (Table 3). The

Table 3. EDS Elemental Composition of Nanoiron (Atomic Percentages), Sample EK35

elements	atomic %
C	51.04 ± 049
O	23.15 ± 0.27
Fe	17.33 ± 0.17
K	6.10 ± 0.04
S	2.39 ± 0.14

iron content of sample EK35 synthesized using plant extract was probably lower than expected from its AMD's content (Figure 1) and lower than that in iron nanoparticles synthesized by a more conventional route owing to the slow exchange of valence electrons between Fe and the polyphenolic constituents of plants (rooibos tea extract in this study), resulting in the formation of a stable iron complex.[36]

3.4. Application of Stabilized Iron Nanoparticles for Decoloration of Orange II Sodium Salt. The effectiveness of iron nanoparticles was evaluated as a Fenton catalyst for decolorizing simulated wastewater containing orange II dye. We varied three parameters in the quest to optimize the decolorization reaction. Figure 7 shows the effects of H_2O_2 concentration (a), pH (b), and nanoiron dosage (c). The latter
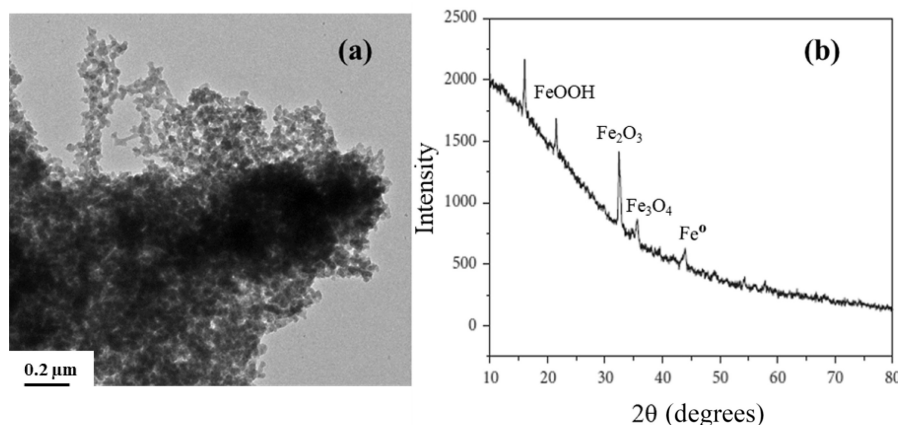

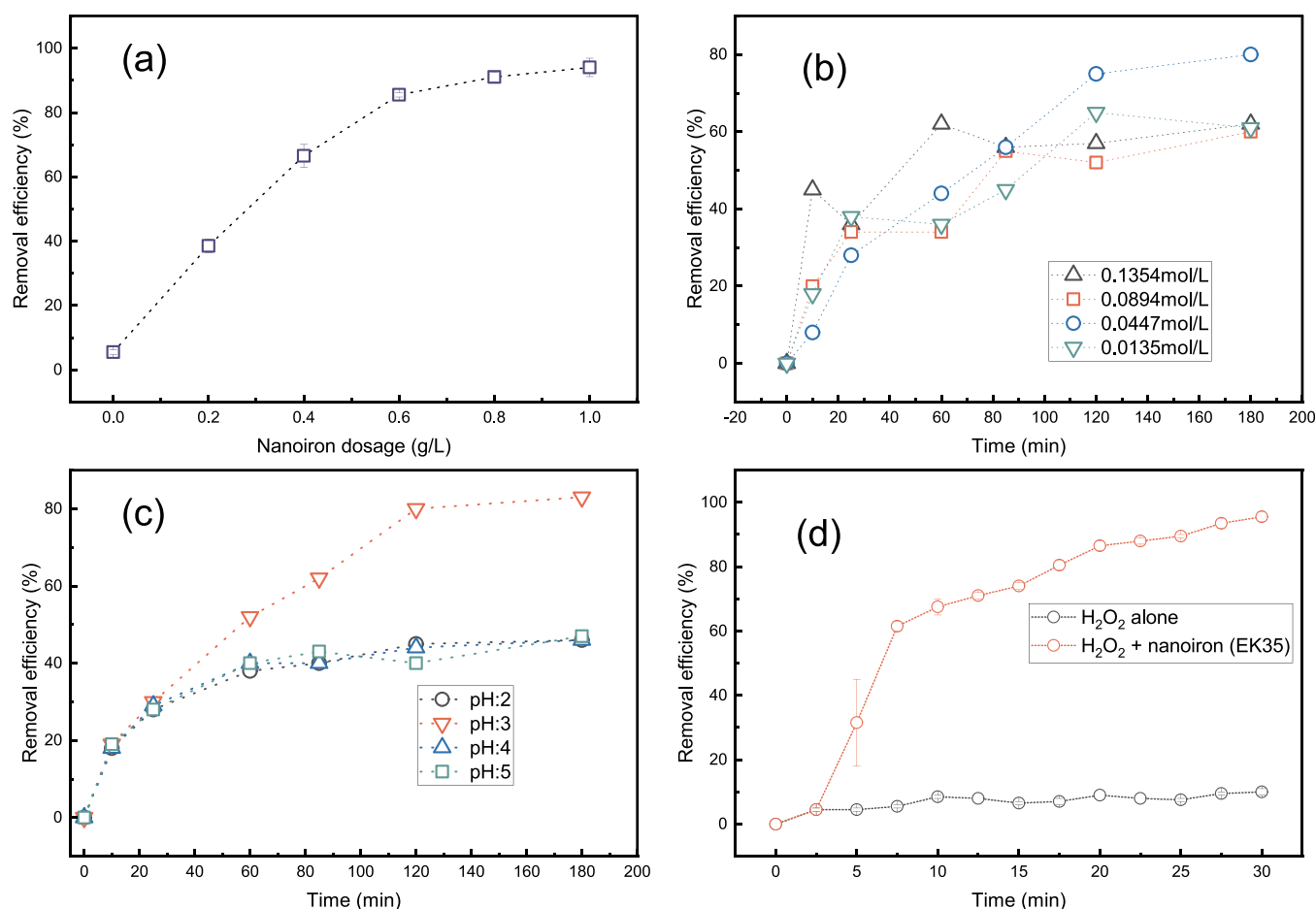**Figure 6.** TEM (a) and XRD patterns (b) of as-prepared EK35.

Figure 7. Decoloration of orange II sodium salt dye with stabilized nanoiron. (a) Effect of nanoiron dosage. (b) Effect of H_2O_2 concentration. (c) Effect of pH. (d) Decoloration at optimum conditions (0.0447 mol/L H_2O_2, pH = 3, and 0.6 g/L of EK35).

was assessed at room temperature (25 ° C), with an initial dye concentration of 50 mg/L, pH of 6, and an H_2O_2 concentration of 0.0894 mol/L. As depicted in Figure 7c, the increase in nanoiron dosage from 0.0 to 0.6 g/L enhanced the oxidative degradation of the dye, which was mainly due to the increase in the number of active sites and improving H_2O_2 decomposition for increased generation of more hydroxyl radicals. However, a further increase from 0.6 to 1.0 g/L did not significantly affect the relative degradation. The reason behind this slow increase at high concentrations may be due to the aggregation of nanoiron particles and the scavenging of hydroxyl radicals through an undesirable reaction. Thus, the nanoiron dosage of 0.6 g/L was chosen as the optimum condition and kept constant while varying H_2O_2 concentrations. Figure 7a reveals that when the concentration of H_2O_2 was set at 0.0135 mol/L, the dye removal efficiency was low (65%) because there was insufficient •OH radicals in aqueous solution. The dye degradation was enhanced to 80% when H_2O_2 concentration further increased to 0.0447 mol/L, mainly due to a higher concentration of •OH radicals. However, dye removal efficiency declined to 60 and 62% at the H_2O_2 concentration of 0.0894 and 0.1354 mol/L, respectively. The main reason behind the decline may be thought to be the scavenging effect of hydroxyl radicals and the inhibition of iron corrosion on the surface of nanoiron by hydrogen peroxide. Hence, 0.0447 mol/ L was chosen as the optimal H_2O_2 concentration for effective oxidative dye degradation. Finally, it has been reported that acidic conditions favor the Fenton-

like process with an optimum pH of 3.5 for the degradation of methyl tertiary butyl ether[42] or between 2 and 4 for the degradation of orange II sodium salts.[36] Therefore, it was not unexpected to confirm those results in our experiments, as depicted in Figure 6c, with an optimum pH of 3.

Employing all optimum parameters, we found that the orange II sodium salt removal was very low and did not exceed 6% when H_2O_2 was used in the absence of nanoiron, as shown in Figure 7d. On the other hand, when nanoiron was added to the simulated dye wastewater solution, the dye removal efficiency reached 95%, demonstrating the importance of the stabilized iron nanoparticles in removing orange II sodium salt regardless of the polyphenol coating and low iron content (~17%).

Furthermore, decoloration of the dye was achieved after 30 min. Few studies have reported such high-efficiency color removal within this short time for unsupported greener nanoparticles without integration with other techniques.[43] This rapid performance may be mainly ascribed to the strong oxidant •OH radicals generated from the oxidation reaction of iron nanoparticle surfaces by transferring two electrons to H_2O_2 (eq 1) to yield Fe^{2+}, which then reacts with H_2O_2 in the Fenton process (eq 2), which is capable of oxidizing organic substrates.

$$Fe^0 + H_2O_2 + 2H^+ \rightarrow Fe^{2+} + 2H_2O \tag{1}$$

$$Fe^{2+} + H_2O_2 \rightarrow Fe^{3+} + \text{•}OH + OH^- \tag{2}$$
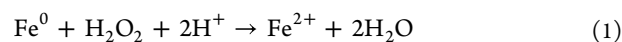
It has been reported that iron nanoparticles synthesized using plant extracts behave primarily as adsorbents rather than reductants. However, the synthesized nanoparticles, which can act as reductants, catalysts, and adsorbents, have been well documented.[44]

The performance of our stabilized nanoiron catalysts was higher than most nZVI reported in the literature for similar tasks. For instance, Bhatti et al.[45] chemically synthesized nZVI using $FeSO_4 \cdot 7H_2O$ and $NaBH_4$. These nanoparticles were then used to treat textile water effluents, and a color removal efficiency of 86−90% under optimum conditions (pH = 3, nZVI = 0.2 g/L, H_2O_2 = 8 mM, and reaction time = 90 min at 40 °C) was achieved despite having a higher iron content of 80.50%.[45] Sravanthi et al.[46] employed a green approach to synthesize nZVI from *Calotropis gigantea* flower extract (both reducing and stabilizing agents) to treat contaminated water. Meanwhile, their nanoparticles possessed average sizes (50−90 nm) that were slightly larger than those synthesized in the current study. Furthermore, dye decoloration and aniline removal hardly exceeded 85% despite the use of sorbent materials in a batch reactor. Employing an alternative synthesis route, Ravikumar et al.,[47] in an attempt to remove methyl orange from textile dye water, obtained Bio-nZVI granules by anaerobic granular sludge under anaerobic conditions. Their catalysts, under optimum conditions, showed removal of up to 99%; it is worth noting that the reaction time was 240 min, 8 times longer than the time required for our catalyst. Lastly, our results are higher than the maximum 90% dye removal reported by several other groups.[41,48,49] The benefit of our study is the short time required to achieve higher removal efficiency and the green synthesis of our catalyst from the reuse of iron in AMD, which is considered both a waste and an environmental hazard.

4. CONCLUSIONS

Iron-rich AMD, a problematic waste effluent, was used as feedstock to produce a value-added product, iron nanoparticles. Rooibos tea was used to reduce Fe^{2+}/Fe^{3+} to Fe^0 from acid mine drainage, replacing the alkaline reagents used in the chemical synthesis methods. To the best of our knowledge, no study has combined waste AMD as a source of iron and rooibos tea extract as a reducing agent and stabilizer instead of chemical synthesis techniques. Thus, as in this study, employing greener methods is a remedial approach. The optimum reaction conditions for synthesizing stabilized iron nanoparticles from acid mine drainage using rooibos tea were ambient temperature (∼ 25 °C), a pH of 6, and a dosage of 5 g/L of rooibos tea for 6 h of reaction time. The synthesized iron nanoparticles were applied as a Fenton-like catalyst for the decoloration of textile dye (orange II sodium salt) and showed a removal efficiency of 94% within 30 min. Compared to nZVI reported in the literature and synthesized by different techniques, our Fenton-like catalyst was very effective with a smaller size, higher removal efficiency, and faster reaction time. Future investigations are necessary to validate the catalyst performance observed in this study. More importantly, other parameters that may further improve the catalyst activity, such as the effects of the dosage of rooibos tea on both the size and the shape of iron nanoparticles, may also be worth studying.

■ AUTHOR INFORMATION

Corresponding Authors

Kashala Fabrice Kapiamba − *Department of Civil, Architectural and Environmental Engineering, Missouri University of Science and Technology, Rolla, Missouri 65401, United States;* ● orcid.org/0000-0003-4958-357X; Email: kapiamba.kashalafabrice@mst.edu

Leslie Petrik − *Environmental and Nanoscience, Chemistry Department, Faculty of Natural Science, University of the Western Cape, Cape Town 8000, South Africa;* Email: lpetrik@uwc.ac.za

Authors

Elyse Kimpiab − *Department of Chemical Engineering, Cape Peninsula University of Technology, Cape Town 7535, South Africa*

Leo Folifac − *Department of Chemical Engineering, Cape Peninsula University of Technology, Cape Town 7535, South Africa*

Oluwaseun Oyekola − *Department of Chemical Engineering, Cape Peninsula University of Technology, Cape Town 7535, South Africa;* ● orcid.org/0000-0002-7198-7346

Complete contact information is available at:
https://pubs.acs.org/10.1021/acsomega.2c01846

Notes

The authors declare no competing financial interest.

■ REFERENCES

(1) Sorensen, P. Mining in South Africa: A Mature Industry? *Int. J. Environ. Stud.* **2011**, *68*, 625−649.

(2) Lum, S. K.; Moyer, B. C. Gross Domestic Product by Industry for 1998 − 2000. *Equals* **2001**, *77*, 84−85.

(3) McCarthy, T. S.; Humphries, M. S. Contamination of the Water Supply to the Town of Carolina, Mpumalanga, January 2012. *S. Afr. J. Sci.* **2013**, *109*, 1−10.

(4) McCarthy, T. S. The Impact of Acid Mine Drainage in South Africa. *S. Afr. J. Sci.* **2011**, *107*, 1−7.

(5) Simate, G. S.; Ndlovu, S. Acid Mine Drainage: Challenges and Opportunities. *J. Environ. Chem. Eng.* **2014**, *2*, 1785−1803.

(6) Hogsden, K. L.; Harding, J. S. Consequences of Acid Mine Drainage for the Structure and Function of Benthic Stream Communities: A Review. *Freshw. Sci.* **2012**, *31*, 108−120.

(7) Naidu, G.; Ryu, S.; Thiruvenkatachari, R.; Choi, Y.; Jeong, S.; Vigneswaran, S. *A Critical Review on Remediation, Reuse, and Resource Recovery from Acid Mine Drainage*; Elsevier Ltd, 2019; Vol. *247*, 1110, DOI: 10.1016/j.envpol.2019.01.085.

(8) Kefeni, K. K.; Msagati, T. A. M.; Mamba, B. B. Acid Mine Drainage: Prevention, Treatment Options, and Resource Recovery: A Review. *J. Cleaner Prod.* **2017**, *151*, 475−493.

(9) Sivaram, N. M.; Gopal, P. M.; Barik, D. *Toxic Waste from Textile Industries*; Elsevier Ltd., 2019. DOI: 10.1016/B978-0-08-102528-4.00004-3.

(10) Samchetshabam, G.; Choudhury, T. G.; Gita, S. Impact of Textile Dyes Waste on Aquatic Environments and Its Treatment Wastewater Management View Project Tribal Sub Plan View Project. 2017, No. December.

(11) Al-Kdasi, A.; Idris, A.; Saed, K.; Guan, C. T. Treatment of Textile Wastewater by Advanced Oxidation Processes− A Review. *Glob. Nest J.* **2004**, *6*, 222−230.

(12) Pearce, C. I.; Lloyd, J. R.; Guthrie, J. T. The Removal of Colour from Textile Wastewater Using Whole Bacterial Cells: A Review. *Dyes Pigm.* **2003**, *58*, 179−196.

(13) Holkar, C. R.; Jadhav, A. J.; Pinjari, D. V.; Mahamuni, N. M.; Pandit, A. B. A Critical Review on Textile Wastewater Treatments: Possible Approaches. *J. Environ. Manage.* **2016**, *182*, 351−366.

(14) Humphries, M. S.; McCarthy, T. S.; Pillay, L. Attenuation of Pollution Arising from Acid Mine Drainage by a Natural Wetland on the Witwatersrand. *S. Afr. J. Sci.* **2017**, *113*, 1−9.

(15) Vadapalli, V. R. K.; Gitari, W. M.; Ellendt, A.; Petrik, L. F.; Balfour, G. Synthesis of Zeolite-P from Coal Fly Ash Derivative and Its Utilisation in Mine-Water Remediation. *S. Afr. J. Sci.* **2010**, *106*, 1−7.

(16) Ouyang, Q.; Kou, F.; Tsang, P. E.; Lian, J.; Xian, J.; Fang, J.; Fang, Z. Green Synthesis of Fe-Based Material Using Tea Polyphenols and Its Application as a Heterogeneous Fenton-like Catalyst for the Degradation of Lincomycin. *J. Cleaner Prod.* **2019**, *232*, 1492−1498.

(17) Yan, Q.; Lian, C.; Huang, K.; Liang, L.; Yu, H.; Yin, P.; Zhang, J.; Xing, M. Constructing an Acidic Microenvironment by MoS2 in Heterogeneous Fenton Reaction for Pollutant Control. *Angew. Chem.* **2021**, *60*, 17155−17163.

(18) Ji, J.; Yan, Q.; Yin, P.; Mine, S.; Matsuoka, M.; Xing, M. Defects on CoS2−x: Tuning Redox Reactions for Sustainable Degradation of Organic Pollutants. *Angew. Chem.* **2021**, *60*, 2903−2908.

(19) Tijani, J. O.; Mouele, M. E. S.; Fatoba, O. O.; Babajide, O. O.; Petrik, L. F. Degradation of Bisphenol-A by Dielectric Barrier Discharge System: Influence of Polyethylene Glycol Stabilized Nano Zero Valent Iron Particles. *Adv. Nat. Sci.: Nanosci. Nanotechnol.* **2017**, *8* (), DOI: 10.1088/2043-6254/aa7714.

(20) Pereao, O.; Bode-Aluko, C.; Fatoba, O.; Laatikainen, K.; Petrik, L. Rare Earth Elements Removal Techniques from Water/Wastewater: A Review. *Desalin. Water Treat.* **2018**, *130*, 71−86.

(21) Malik, P. K.; Saha, S. K. Oxidation of Direct Dyes with Hydrogen Peroxide Using Ferrous Ion as Catalyst. *Sep. Purif. Technol.* **2003**, *31*, 241−250.

(22) Shahwan, T.; Abu Sirriah, S.; Nairat, M.; Boyaci, E.; Eroĝlu, A. E.; Scott, T. B.; Hallam, K. R. Green Synthesis of Iron Nanoparticles and Their Application as a Fenton-like Catalyst for the Degradation of Aqueous Cationic and Anionic Dyes. *Chem. Eng. J.* **2011**, *172*, 258−266.

(23) Mukherjee, R.; Kumar, R.; Sinha, A.; Lama, Y.; Saha, A. K. A Review on Synthesis, Characterization, and Applications of Nano Zero Valent Iron (NZVI) for Environmental Remediation. *Crit. Rev. Environ. Sci. Technol.* **2016**, *46*, 443−466.

(24) Sun, Y.; Li, J.; Huang, T.; Guan, X. The Influences of Iron Characteristics, Operating Conditions and Solution Chemistry on Contaminants Removal by Zero-Valent Iron: A Review. *Water Res.* **2016**, *100*, 277−295.

(25) Stefaniuk, M.; Oleszczuk, P.; Ok, Y. S. Review on Nano Zerovalent Iron (NZVI): From Synthesis to Environmental Applications. *Chem. Eng. J.* **2016**, *287*, 618−632.

(26) Fazlzadeh, M.; Rahmani, K.; Zarei, A.; Abdoallahzadeh, H.; Nasiri, F.; Khosravi, R. A Novel Green Synthesis of Zero Valent Iron Nanoparticles (NZVI) Using Three Plant Extracts and Their Efficient Application for Removal of Cr(VI) from Aqueous Solutions. *Adv. Powder Technol.* **2017**, *28*, 122−130.

(27) Abdelfatah, A. M.; Fawzy, M.; Eltaweil, A. S.; El-Khouly, M. E. Green Synthesis of Nano-Zero-Valent Iron Using Ricinus Communis Seeds Extract: Characterization and Application in the Treatment of Methylene Blue-Polluted Water. *ACS Omega* **2021**, *6*, 25397−25411.

(28) Lem, O.; Yoon, S.; Bae, S.; Lee, W. The Enhanced Reduction of Bromate by Highly Reactive and Dispersive Green Nano-Zerovalent Iron (G-NZVI) Synthesized with Onion Peel Extract. *RSC Adv.* **2021**, *11*, 5008−5018.

(29) Le, N. T.; Dang, T. D.; Hoang Binh, K.; Nguyen, T. M.; Xuan, T. N.; La, D. D.; Kumar Nadda, A.; Chang, S. W.; Nguyen, D. D. Green Synthesis of Highly Stable Zero-Valent Iron Nanoparticles for Organic Dye Treatment Using Cleistocalyx Operculatus Leaf Extract. *Sustain. Chem. Pharm.* **2022**, *25*, No. 100598.

(30) Rashtbari, Y.; Sher, F.; Afshin, S.; Hamzezadeh Bahrami, A.; Ahmadi, S.; Azhar, O.; Rastegar, A.; Ghosh, S.; Poureshgh, Y. Green Synthesis of Zero-Valent Iron Nanoparticles and Loading Effect on Activated Carbon for Furfural Adsorption. *Chemosphere* **2022**, *287*, No. 132114.

(31) Kalombe, R. M.; Ojumu, T. V.; Katambwe, V. N.; Nzadi, M.; Bent, D.; Nieuwoudt, G.; Madzivire, G.; Kevern, J.; Petrik, L. F. Treatment of Acid Mine Drainage with Coal Fly Ash in a Jet Loop Reactor Pilot Plant. *Miner. Eng.* **2020**, *159*, No. 106611.

(32) Benzie, I. F. F.; Strain, J. J. The Ferric Reducing Ability of Plasma (FRAP) as a Measure of "Antioxidant Power:" The FRAP Assay. *Anal. Biochem.* **1996**, *239*, 70−76.

(33) Kuang, Y.; Wang, Q.; Chen, Z.; Megharaj, M.; Naidu, R. Heterogeneous Fenton-like Oxidation of Monochlorobenzene Using Green Synthesis of Iron Nanoparticles. *J. Colloid Interface Sci.* **2013**, *410*, 67−73.

(34) Hoag, G. E.; Collins, J. B.; Holcomb, J. L.; Hoag, J. R.; Nadagouda, M. N.; Varma, R. S. Degradation of Bromothymol Blue by "greener" Nano-Scale Zero-Valent Iron Synthesized Using Tea Polyphenols. *J. Mater. Chem.* **2009**, *19*, 8671−8677.

(35) Liu, A.; Zhang, W. X. Fine Structural Features of Nanoscale Zero-Valent Iron Characterized by Spherical Aberration Corrected Scanning Transmission Electron Microscopy (Cs-STEM). *Analyst* **2014**, *139*, 4512−4518.

(36) Badmus, K. O.; Coetsee-Hugo, E.; Swart, H.; Petrik, L. Synthesis and Characterisation of Stable and Efficient Nano Zero Valent Iron. *Environ. Sci. Pollut. Res.* **2018**, *25*, 23667−23684.

(37) Taha, M. R.; Ibrahim, A. H. Characterization of Nano Zero-Valent Iron (NZVI) and Its Application in Sono-Fenton Process to Remove COD in Palm Oil Mill Effluent. *J. Environ. Chem. Eng.* **2014**, *2*, 1−8.

(38) Njagi, E. C.; Huang, H.; Stafford, L.; Genuino, H.; Galindo, H. M.; Collins, J. B.; Hoag, G. E.; Suib, S. L. Biosynthesis of Iron and Silver Nanoparticles at Room Temperature Using Aqueous Sorghum Bran Extracts. *Langmuir* **2011**, *27*, 264−271.

(39) Giasuddin, A. B. M.; Kanel, S. R.; Choi, H. Adsorption of Humic Acid onto Nanoscale Zerovalent Iron and Its Effect on Arsenic Removal. *Environ. Sci. Technol.* **2007**, *41*, 2022−2027.

(40) Huang, L.; Luo, F.; Chen, Z.; Megharaj, M.; Naidu, R. Green Synthesized Conditions Impacting on the Reactivity of Fe NPs for the Degradation of Malachite Green. *Spectrochim. Acta, Part A* **2015**, *137*, 154−159.

(41) Wang, T.; Lin, J.; Chen, Z.; Megharaj, M.; Naidu, R. Green Synthesized Iron Nanoparticles by Green Tea and Eucalyptus Leaves Extracts Used for Removal of Nitrate in Aqueous Solution. *J. Cleaner Prod.* **2014**, *83*, 413−419.

(42) Samaei, M. R.; Maleknia, H.; Azhdarpoor, A. Effects of PH on the Kinetics of Methyl Tertiary Butyl Ether Degradation by Oxidation Process (H2O2/Nano Zero-Valent Iron/Ultrasonic). *Jundishapur J. Heal. Sci.* **2015**, *7*, 4−9.

(43) Raman, C. D.; Kanmani, S. Textile Dye Degradation Using Nano Zero Valent Iron: A Review. *J. Environ. Manage.* **2016**, *177*, 341−355.

(44) Kim, D. G.; Hwang, Y. H.; Shin, H. S.; Ko, S. O. Kinetics of Nitrate Adsorption and Reduction by Nano-Scale Zero Valent Iron (NZVI): Effect of Ionic Strength and Initial PH. *KSCE J. Civ. Eng.* **2016**, *20*, 175−187.

(45) Bhatti, H. N.; Iram, Z.; Iqbal, M.; Nisar, J.; Khan, M. I. Facile Synthesis of Zero Valent Iron and Photocatalytic Application for the Degradation of Dyes. *Mater. Res. Express* **2020**, *7* (), DOI: 10.1088/2053-1591/ab66a0.

(46) Sravanthi, K.; Ayodhya, D.; Yadgiri Swamy, P. Green Synthesis, Characterization of Biomaterial-Supported Zero-Valent Iron Nanoparticles for Contaminated Water Treatment. *J. Anal. Sci. Technol.* **2018**, *9* (), DOI: 10.1186/s40543-017-0134-9.

(47) Ravikumar, K. V. G.; Santhosh, S.; Sudakaran, S. V.; Nancharaiah, Y. V.; Mrudula, P.; Chandrasekaran, N.; Mukherjee, A. Biogenic Nano Zero Valent Iron (Bio-NZVI) Anaerobic Granules for Textile Dye Removal. *J. Environ. Chem. Eng.* **2018**, *6*, 1683−1689.

(48) Lin, Z.; Weng, X.; Owens, G.; Chen, Z. Simultaneous Removal of Pb(II) and Rifampicin from Wastewater by Iron Nanoparticles Synthesized by a Tea Extract. *J. Cleaner Prod.* **2020**, 242.

(49) Gottimukkala, K. S. V. Green Synthesis of Iron Nanoparticles Using Green Tea Leaves Extract. *J. Nanomed. Biother. Discov.* **2017**, *07*, 1−4.

📖 Recommended by ACS

Synthetic Ilmenite (FeTiO$_3$) Nanoparticles as a Heterogeneous Electro-Fenton Catalyst for the Degradation of Tetracycline in Wastewater

Charles Muzenda, Omotayo A. Arotiba, *et al.*

JULY 26, 2022
INDUSTRIAL & ENGINEERING CHEMISTRY RESEARCH   READ 🗗

Nano-sized Zero-Valent Iron Coupled with Sulfidation and Ferrous Implantation Enhances the Reduction–Oxidation Removal of Iodinated Contras...

Guannan Zhou, Yang Mu, *et al.*

AUGUST 11, 2021
ACS ES&T WATER   READ 🗗

Role of Gallic Acid in the Synthesis of Carbon-Encapsulated Iron Nanoparticles by Hydrothermal Carbonization: Selecting Iron Oxide Composition

Rubén Correcher, Andrés Fullana, *et al.*

OCTOBER 26, 2021
ACS OMEGA   READ 🗗

Copper Nanostructure Genesis via Galvanic Replacement and Kirkendall Growth from Nanoscale Zero-Valent Iron

Airong Liu, Weixian Zhang, *et al.*

JULY 25, 2022
ACS ES&T WATER   READ 🗗

Get More Suggestions >